Sub-Nanometer Level Size Tuning of a Monodisperse Nanoparticle Array Via Block Copolymer Lithography

Dong Ok Shin, Duck Hyun Lee, Hyoung-Seok Moon, Seong-Jun Jeong, Ju Young Kim, Jeong Ho Mun, Heesook Cho, Soojin Park, and Sang Ouk Kim**

The fabrication and catalytic application of a size-tunable monodisperse nanoparticle array enabled by block copolymer lithography is demonstrated. Highly uniform vertical cylinder nanodomains are achieved in poly(styrene-*block*-4-vinylpyridine) (PS-*b*-P4VP) diblock copolymer thin-films by solvent annealing. The prominent diffusion of the anionic metal complexes into the protonated P4VP cylinder nanodomains occurs through specific electrostatic interactions in a weakly acidic aqueous solution. This well-defined diffusion with nanoscale confinement enables preparation of the laterally ordered monodisperse nanoparticle array with sub-nanometer level precise size tuning. The controlled growth of monodisperse nanoparticle arrays is proven by their catalytic use for vertical carbon nanotube (CNT) growth via plasma enhanced chemical vapor deposition (PECVD). Since the size of the catalyst particles is the decisive parameter for the diameters and wall-numbers of CNTs, the highly selective growth of double-walled or triple-walled CNTs could be accomplished using monodisperse nanoparticle arrays.

1. Introduction

Nanoscale particles exhibit size-dependent electric,[1,2] magnetic,[3,4] chemical,[5] optical,[6,7] and catalytic[8,9] properties enforced by nanoscale quantum confinement and an ultra-large surface area. Patterning of nanoparticles into 2D arrays has attracted enormous research interest due to the potential applications to sensors,[10,11] magnetic data storage,[12] flash memory,[13] catalysis,[14] and so on. Nevertheless, despite the enormous progress in the nanoparticle synthesis, precise positioning and immobilization of nanoparticles on a suitable substrate surface remains a formidable technological challenge. In this regard, the controlled deposition of nanopatterned particles at a desired substrate is highly anticipated. If the precise tunability of the deposition rate is acquired, the extraordinary characteristics of the size-tunable nanoparticle array would enable the aforementioned applications.

Block copolymer lithography has evolved into a viable nanolithography to overcome the intrinsic resolution limit of conventional photolithography.[15–23] The parallel self-assembly of microphase separated block copolymer nanodomains enables the scalable production of a sub-30-nm scale periodic nanolithographic mask over an arbitrary large area. Furthermore, recent progress of directed assembly utilizing an external field[24] or a chemical or topographic prepattern[25,26] accomplishes laterally ordered nanopatterns over a large area. However, the intrinsic polydispersity of self-assembled nanodomains has been the technological challenge for creating monodisperse nanopatterned morphology.[16,27–29] Moreover, successful demonstration of a size-tunable pattern transfer strategy has rarely been achieved from block copolymer lithography thus far.

In this work, we establish a straightforward strategy for the sub-nanometer level size tuning of a monodisperse nanoparticle array via block copolymer lithography. The uniformity of structure-directing block copolymer morphology as well as highly specific metal deposition mediated by electrostatic interactions are suggested as two crucial requirements for the monodisperse nanoparticle array deposition with the ultrafine size tunability.

2. Results and Discussion

Figure 1a schematically describes the overall process. An amphiphilic poly(styrene-block-4-vinylpyridine) (PS-*b*-P4VP) (24.0 kg mol^{-1} for PS block and 9.5 kg mol^{-1} for P4VP block) block copolymer thin-film was self-assembled into the vertical P4VP nanocylinder array in the PS matrix immediately after spin casting from a toluene:tetrahydrofuran (THF) solvent mixture onto an arbitrary substrate (Supporting Information, Figure S1). Subsequently, solvent annealing under the toluene:THF mixture vapor gradually enhanced the lateral ordering of cylinder nanodomains with time.[18,30–32] Along with the lateral ordering, the size of the cylinder domains became

D. O. Shin, D. H. Lee, H.-S. Moon, Dr. S.-J. Jeong, J. Y. Kim, J. H. Mun, Prof. S. O. Kim
Department of Materials Science and Engineering
KAIST Institute for the Nanocentury
KAIST, Daejeon 305–701, Republic of Korea
E-mail: sangouk.kim@kaist.ac.kr
H. Cho, Prof. S. Park
School of Energy Engineering
Ulsan National Institute of Science and Technology
Ulsan, 689–798, Republic of Korea
E-mail: spark@unist.ac.kr

DOI: 10.1002/adfm.201001396

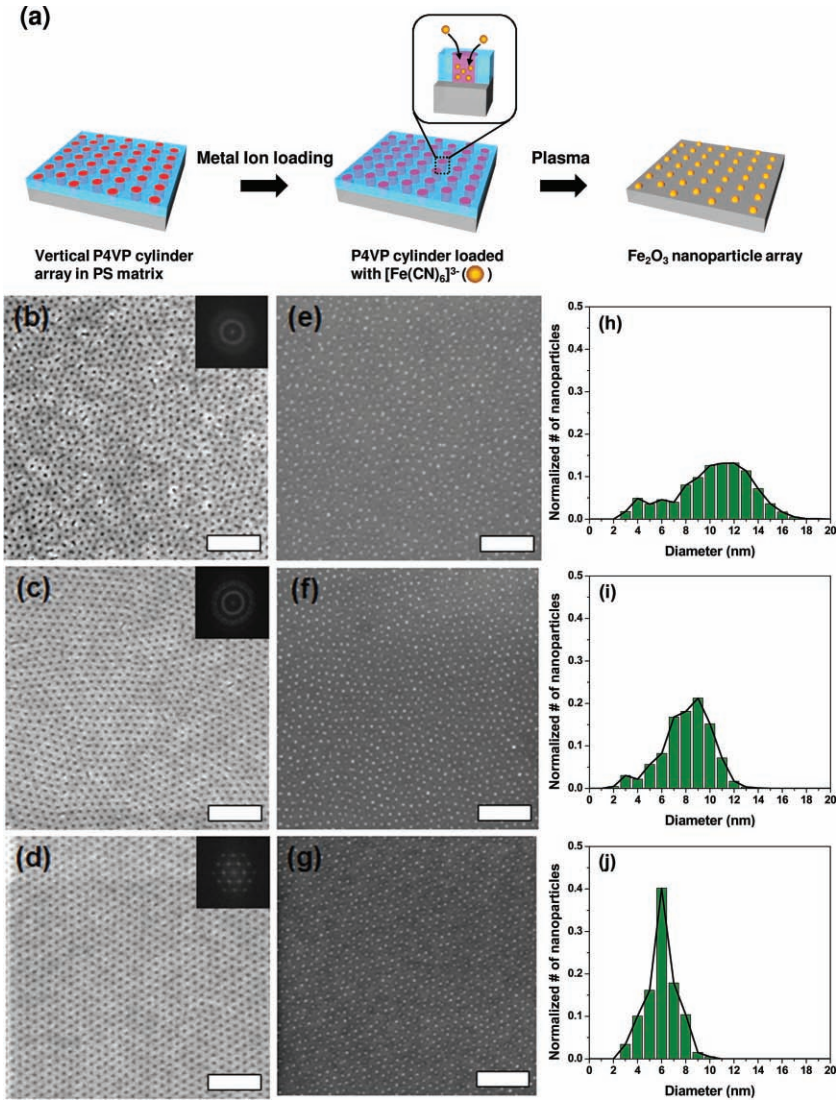

Figure 1. a) Schematic procedure for sub-nanometer level size tuning of a monodisperse nanoparticle array. A block copolymer thin-film is self-assembled into vertical P4VP cylinders surrounded by a PS matrix. The P4VP block becomes loaded with iron complexes in aqueous solution. Oxygen plasma treatment leaves a monodisperse nanoparticle array replicating the parent block copolymer morphology. SEM images of b) as-cast, c) 2 h solvent-annealed, and d) 5 h solvent-annealed PS-*b*-P4VP films on a silicon substrate. Insets are FFT images. e–g) SEM images of Fe_2O_3 nanoparticle arrays of the corresponding PS-*b*-P4VP films from (b–d). h–j) Statistical size distribution of Fe_2O_3 nanoparticle arrays from (e–g). The white scale bars represent 200 nm.

highly uniform. Approximately 5 h of annealing generated a laterally ordered hexagonal cylinder array with a remarkably narrow size distribution. The highly ordered block copolymer thin-film deposited onto a substrate was then immersed in an aqueous solution of 1 mM $K_3[Fe(CN)_6]$:0.1% HCl. The anionic complexes of $Fe(CN)_6^{-3}$ were specifically associated with the protonated pyridine nitrogen in the P4VP cylinder nanodomains. Oxygen plasma treatment over the entire area effectively removed the organic block polymer template, while monodisperse iron oxide (Fe_2O_3) nanoparticle arrays were left at the locations of the P4VP cylinders.[33,34] The nanoparticle size could be precisely tuned at the sub-nanometer level with the iron complex loading time in the aqueous solution. An Fe_2O_3 nanoparticle array was prepared in this work due to the catalytic functionality for carbon nanotube (CNT) growth. In addition to $K_3[Fe(CN)_6]$, any other ionic metal complexes can be utilized to generate different metal nanoparticle arrays on an arbitrary substrate surface.

Figure 1b–d show scanning electron microscopy (SEM) images of as-spun (Figure 1b) and solvent-annealed (Figure 1c,d) PS-*b*-P4VP thin-films on silicon substrates. The nanocylinders were vertically oriented in the as-spun film (Figure 1b) due to the highly directional solvent evaporation during spin-casting. However, the lateral ordering of the cylinders was poor and their size distribution was significantly broad (Figure 1b). The lateral ordering and size uniformity could be greatly improved after solvent annealing in the toluene:THF (20:80, v:v) mixture at room temperature. While the 2 h annealed sample revealed hexagonal ordering with relatively small grain sizes (Figure 1c), the 5 h annealed sample showed well-developed hexagonal ordering with a large grain size (Figure 1d). The fast Fourier transforms (FFTs) also reflect this remarkable enhancement in lateral ordering (Figure 1b–d, insets). The six-point spots with strong multiple higher order reflections, which are characteristic of long-range order, represent the highly ordered hexagonal packing (Figure 1d, inset).

Figure 1e–g show Fe_2O_3 nanoparticle arrays prepared by immersing the as-spun and solvent-annealed block copolymer templates in an aqueous solution containing ionic metal complexes for 1 min. Since P4VP vertical cylinders are directly exposed to the aqueous ion complex solution, anionic metal complexes are readily associated with the protonated pyridine units in a weak acidic condition.[35] Therefore, the resulting Fe_2O_3 nanoparticle arrays exactly replicated the block copolymer template morphology. The particles prepared from the as-spun or insufficiently annealed film revealed large diameters and broad size distributions (10.84 nm ± 2.98 nm for the as-spun film and 8.40 nm ± 1.79 nm for the 2 h annealed film). In contrast, the particles from a well-developed template had small sizes and a narrow size distribution of the cylinders (6.03 nm ± 1.0 nm), in addition to greatly enhanced lateral ordering (Figure 1h–j). **Table 1** summarizes the characteristic nanoscale dimensions of block copolymer nanotemplates and the resultant nanoparticle arrays in Figure 1. The mean diameter of nanoparticles was slightly less than the block copolymer cylinder diameter due to the particle densification during the removal of the block copolymer template by plasma treatment.

Table 1. Characteristic nanoscale dimensions of solvent-annealed block copolymer films and the resulting iron oxide nanoparticle arrays in Figure 1.

Annealing time	Block copolymer template		Iron oxide nanoparticle array	
	Mean diameter (nm)	Average center-to-center distance (nm)	Mean diameter (nm)	Average center-to-center distance (nm)
As-spun	11.04 ± 3.9	24.58 ± 4.6	10.84 ± 2.98	25.38 ± 6.1
2 h	10.35 ± 2.3	22.39 ± 2.6	8.40 ± 1.79	23.95 ± 4.5
5 h	9.01 ± 1.2	19.23 ± 1.3	6.03 ± 1.0	19.71 ± 1.7

The series of SEM images in **Figure 2**a shows the evolution of the nanoparticle arrays prepared from a 5 h solvent annealed template as a function of ionic complex loading time. The size of the highly monodisperse nanoparticles gradually increased with loading time. This precise particle size tunability on a sub-nanometer scale was attained at the relatively low concentration of 1 mM for $K_3[Fe(CN)_6]$. The variation of the mean diameter and height is plotted against the loading time in Figure 2b (Supporting Information, Figure S2). The growth rate was fast in the short loading time but gradually became saturated. The growth behavior could be fit with a typical power law curve, At^{α}. Least-square fits result in exponent, α, values of 0.16 for the diameter and 0.39 for the height. This prominent low value is due to the low concentration of ion complexes as well as the confined diffusion through P4VP nanoscale cylinders. The surrounding PS matrix effectively acted as the barrier for lateral diffusion of ion complexes. Nevertheless, the prolonged loading time caused the coalescence of nanoparticles (see Supporting Information, Figure S3). Figure 2c shows the characteristic X-ray photoelectron spectroscopy (XPS) spectrum of the Fe_2O_3 nanoparticle array obtained after oxygen plasma treatment. The Fe-$2p_{3/2}$ peak at 710.5 eV confirms that Fe is present in the Fe_2O_3 state.[36]

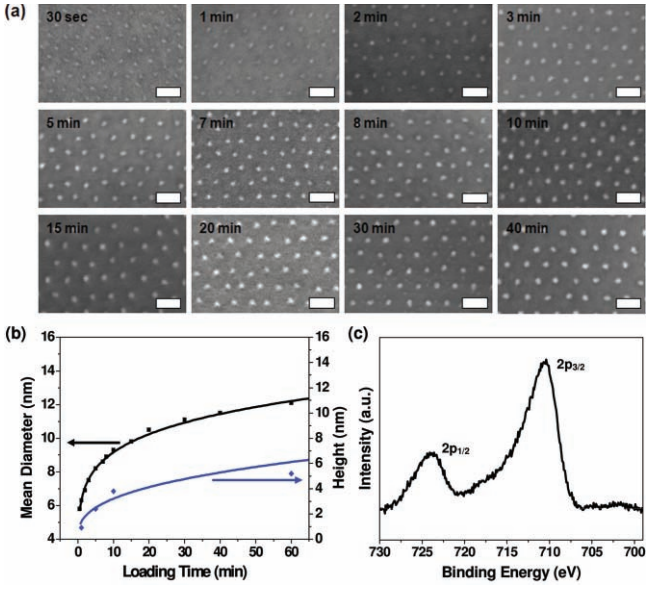

Figure 2. a) A series of SEM images of the monodisperse Fe_2O_3 nanoparticle arrays as a function of ion complex loading time. The white scale bars represent 50 nm. b) The mean diameter and height plotted against loading time (0–60 min). Solid lines are fit to At^{α} ($A = 6.34$, $\alpha = 0.16$ for mean diameter, $A = 1.1$, $\alpha = 0.39$ for height). c) XPS data from Fe-$2p_{1/2}$ (724.1 eV) and $2p_{3/2}$ (710.5 eV) peaks of Fe_2O_3 nanoparticles.

The catalytic functionality of the monodisperse nanoparticle arrays was investigated via catalytic CNT growth. Among various CNT synthetic approaches, plasma enhanced chemical vapor deposition (PECVD) was employed for the highly oriented vertical growth.[37] The PECVD also enabled low-temperature growth below 600 °C, which is greatly advantageous for device integration. The as-prepared Fe_2O_3 particle arrays were thermally reduced into metallic Fe particles before CNT growth. A slow stream of a hydrogen (H_2), ammonia (NH_3), and acetylene (C_2H_2) gas mixture fostered high-yield growth of vertical CNTs (**Figure 3**a). This high-yield growth signifies the high purity and functionality of the prepared nanoparticle array. The 26.7-μm-tall

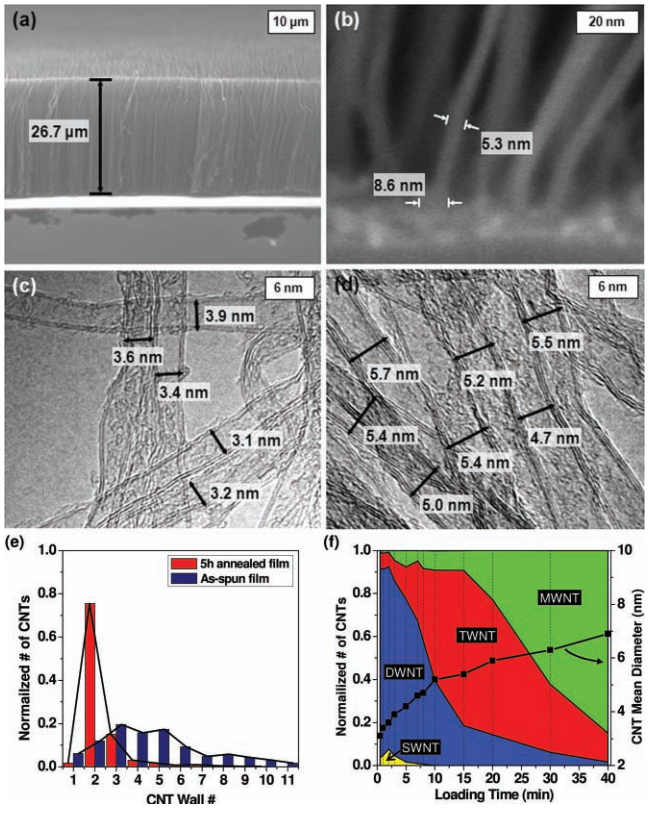

Figure 3. a) Cross-sectional SEM images of vertical CNTs. b) High-magnification SEM image of vertical CNTs grown from nanoparticles catalysts. HRTEM images of c) double-walled and d) triple-walled CNTs grown from size-controlled nanoparticle catalysts. e) Statistical wall-number analysis of CNTs grown from as-spun and 5 h annealed block copolymer template. f) The relative fractions of CNTs with single, double, triple, and multiple walls plotted against ion loading time. The mean diameter of CNTs is also plotted against the loading time.

CNTs were grown in 1 min using optimized conditions. Figure 3b shows the high-magnification SEM image of the bottom part of the CNTs. The CNT diameter of ≈5.3 nm was approximately two-thirds of the catalyst particle diameter of ≈8.6 nm. Figure 3c,d show the high-resolution transmission electron microscopy (TEM) images of the CNTs grown from the monodisperse catalyst arrays, which had average diameters of 5.8 and 9.9 nm. The narrow distributions of the CNT diameter and graphitic wall-number are attributed to the monodispersity of catalyst particles. While ≈88% of the CNTs grown from 5.6 nm catalyst particles were double-walled (Figure 3c), ≈72% of CNTs grown from 9.9 nm particles were triple-walled (Figure 3d). Figure 3e compares the statistical wall-number distributions of the CNTs prepared from the as-spun and 5 h annealed block copolymer templates. The loading time of the ion complexes was maintained at 5 min. Since the nanoparticle arrays from the as-spun template had a broad size distribution, the resultant CNTs also revealed a broad wall-number distribution. In contrast, the wall-number of CNTs obtained from a 5 h annealed block copolymer template demonstrated a much narrower distribution. Figure 3f presents the relative fractions of single-walled CNTs (SWNTs), double-walled CNTs (DWNTs), triple-walled CNTs (TWNTs), and more than four walled CNTs (multiwalled, MWNTs), prepared from a 5 h annealed block copolymer template, plotted against the ion complex loading time. The relative fraction of each wall-number varied along with the catalyst size as a function of the loading time. We note that in our CNT growth under an NH_3 environment, the growth of SWNTs is suppressed, even from the smallest catalyst, due to the nitrogen doping effect.[37] In Figure 3f, the mean diameter of the CNTs is also plotted against the ion loading time. The growth trend was similar to the catalyst particle growth, confirming that the CNT diameter is closely related to the catalyst particle size (Supporting Information, Table S1).

Our size-tunable nanoparticle deposition allows for the hierarchical patterning of the catalyst and corresponding CNT arrays. As described in **Figure 4**a, nanoparticle deposition does not occur without the block copolymer template. Masked oxygen plasma etching was employed to generate hierarchically patterned block copolymer templates. The resultant morphology of the vertical CNTs exactly replicated the etching mask. The cross-sectional SEM image shows that CNTs are absent in the etched area (Figure 4b). Figure 4c–e show the SEM images of the patterned CNT arrays prepared from hexagonal and square masks. Such hierarchically patterned vertical CNT arrays with tunable diameters and wall-numbers offer great potential for various applications, such as field emitting devices, where the field screening effect caused by the proximity of neighboring tubes can be greatly relieved by the hierarchical patterning.[38–41]

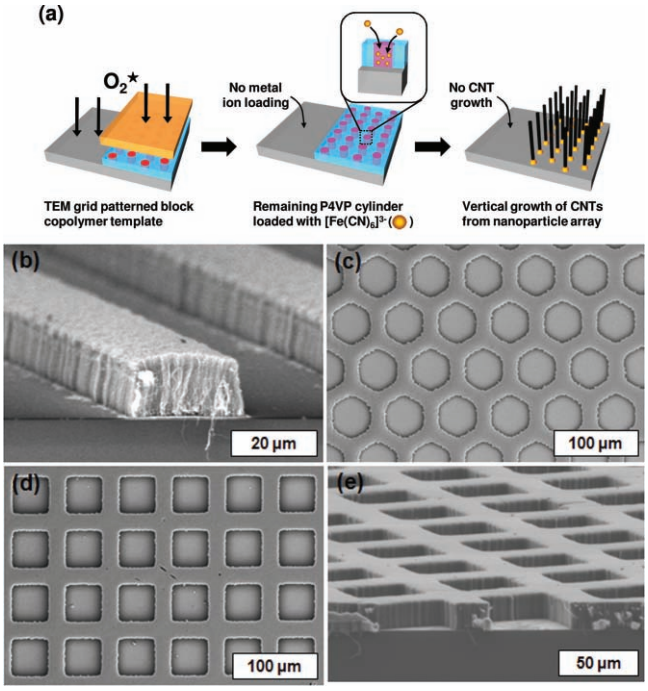

Figure 4. The hierachical patterning of nanoparticle arrays and the corresponding vertical CNTs. a) Schematic description of the hierarchical patterning. b) Cross-sectional SEM image of the vertical CNTs prepared with parallel grid etching mask. c) Plain-view SEM image of the vertical CNTs prepared with hexagonal grid etching mask. d) Plain-view and e) cross-sectional SEM images of vertical CNTs prepared with square grid etching mask.

3. Conclusions

The size-tunable monodisperse nanoparticle array deposition via block copolymer lithography was demonstrated. Highly ordered vertical cylinder nanodomains were achieved in a PS-*b*-P4VP block copolymer thin-film by solvent annealing. Upon immersion in aqueous ionic metal complex solution, the anionic metal complexes diffuse into the P4VP cylinder cores, mediated by highly specific electrostatic interactions. This well-defined diffusion with nanoscale confinement enabled the sub-nanometer level precise size tuning of a laterally ordered monodisperse nanoparticle array. The catalytic functionality of the monodisperse nanoparticle array was proven by vertical CNT growth via catalytic PECVD. The sub-nanometer level size tuning of catalyst nanoparticles enabled the highly selective growth of wall-number-selected vertical CNTs.

4. Experimental Section

Materials: An asymmetric block copolymer, polystyrene-*block*-poly(4-vinylpyridine) (PS-*b*-P4VP, molecular weight: 24 kg mol^{-1} for PS, 9.5 kg mol^{-1} for P4VP) was purchased from Polymer Source (Montreal, Canada). Potassium ferricyanide ($K_3Fe(CN)_6$) was acquired from Strem Chemicals (Orwell, UK). Pure ammonia and acetylene gases were purchased from Showa Denko K.K. (Tokyo, Japan) and Kyungin Chemical Industrial (Incheon, Korea), respectively.

Deposition of metal nanoparticle arrays: A silicon wafer was immersed in a piranha solution (7:3 mixture of H_2SO_4 and H_2O_2) for 1 h at 110 °C and then washed several times with deionized water. PS-*b*-P4VP block copolymers (0.5 wt%) were dissolved in toluene/THF solvent mixtures (80:20, v:v). The 25-nm-thick PS-*b*-P4VP thin-films were spin-coated from a 0.5 wt% toluene:THF solution onto the cleaned silicon wafers. The as-spun film was solvent annealed in a small closed vessel. A homogeneous liquid mixture of toluene and THF (toluene:THF 20:80 v:v) was injected into the vessel. The small vessel was saturated with the spontaneously evaported solvent vapor in several minutes at a room

temperature (25 °C ± 2 °C). The volume ratio of the toluene vapor and THF vapor was inconsistent with that of liquid mixture due to different vapor pressures of toluene and THF. Then, the as-spun films were annealed for 0 to ≈5 h to develop the lateral ordering of the cylinder nanodomains. The solvent annealed samples were then immersed in an aqueous solution of 1 mM $K_3[Fe(CN)_6]$: 0.1% HCl for a given loading time. After metal ion loading, the samples were rinsed with deionized water for several times to remove excess amounts of metal ions and dried with N_2 gas. The oxygen plasma treatment removed polymer template and left the Fe_2O_3 nanoparticle arrays on the silicon substrate.

PECVD growth of vertical CNTs: CNT growth was carried out via the catalytic PECVD method. The substrate was heated to 600 °C under a mixture of hydrogen and ammonia gas flow (chamber pressure: 0.4 torr). The H_2:NH_3 contents were maintained at 80:20 vol% and the total flow rate of the environmental gas was fixed at 100 sccm (standard cubic centimeters per minute). When the substrate temperature reached 600 °C, the substrate was annealed (usually for less than 2 min) to reduce Fe_2O_3 nanoparticles into metallic Fe. The chamber pressure was increased to 5 torr and a direct current (DC) plasma was activated with an anode DC voltage of 470 V relative to the grounded substrate. Slow, streaming acetylene gas at a flow rate of 5 sccm for about 1 to 2 min fostered dense vertical CNTs.

Characterization: The nanoscale morphology of block copolymer thin-films, metal nanoparticle arrays, and the vertical CNT arrays were characterized using a Hitachi S-4800 FE-SEM. A high-resolution transmission electron microscope (HRTEM; Philips Tecnai F20) was used to statistically analyze the diameters and the wall-numbers of the CNTs. For reliable statistics, the diameters and wall-numbers of ≈250 to 350 CNTs were measured for each vertical CNT array. XPS measurements were performed using an ESCA 2000 system (Thermo VG Scientific). The height profiles of the nanoparticle arrays were analyzed using atomic force microscopy (AFM; Veeco, USA) in a tapping mode.

Supporting Information

Supporting Information is available from the Wiley Online Library or from the author.

Acknowledgements

This work was supported by the National Research Laboratory Program (R0A-2008–000-20057–0), the World Class University (WCU) program (R32–2008-000–10051-0, R31–2008-000–20012-0), a Platform Project grant (10033636–2009-11), and the Fundamental R&D Program for Core Technology of Materials funded by the Korean government.

Received: July 12, 2010
Revised: August 2, 2010
Published online: October 27, 2010

[1] G. Schmid, U. Simon, *Chem. Commun.* **2005**, *6*, 697.
[2] M. C. Beard, G. M. Turner, J. E. Murphy, O. I. Micic, M. C. Hanna, A. J. Nozik, C. A. Schmuttenmaer, *Nano Lett.* **2003**, *3*, 1695.
[3] S. Sun, C. B. Murray, D. Weller, L. Folks, A. Moser, *Science* **2000**, *287*, 1989.
[4] A. Imre, G. Csaba, L. Ji, A. Orlov, G. H. Bernstein, W. Porod, *Science* **2006**, *311*, 205.
[5] V. P. Zhdanov, B. Kasemo, *J. Phys.: Condens. Matter* **2004**, *16*, 7131.
[6] C. Langhammer, Z. Yuan, I. Zori , B. Kasemo, *Nano Lett.* **2006**, *6*, 833.
[7] P. P. Pompa, L. Martiradonna, A. Della Torre, F. Della Sala, L. Manna, M. De Vittorio, F. Calabi, R. Cingolani, R. Rinaldi, *Nat. Nanotechnol.* **2006**, *1*, 126.
[8] R. Narayanan, M. A. El-Sayed, *Nano Lett.* **2004**, *4*, 1343.
[9] D. Takagi, Y. Homma, H. Hibino, S. Suzuki, Y. Kobayashi, *Nano Lett.* **2006**, *6*, 2642.
[10] D. O. Shin, J.-R. Jeong, T. H. Han, C. M. Koo, H.-J. Park, Y. T. Lim, S. O. Kim, *J. Mater. Chem.* **2010**, **20**, 7241.
[11] A. J. Haes, W. P. Hall, L. Chang, W. L. Klein, R. P. Van Duyne, *Nano Lett.* **2004**, *4*, 1029.
[12] K. Naito, H. Hieda, M. Sakurai, Y. Kamata, K. Asakawa, *IEEE Trans. Magn.* **2002**, *38*, 1949.
[13] J.-S. Lee, J. Cho, C. Lee, I. Kim, J. Park, Y.-M. Kim, H. Shin, J. Lee, F. Caruso, *Nat. Nanotechnol.* **2007**, *2*, 790.
[14] N. C. Bigall, M. Reitzig, W. Naumann, P. Simon, K.-H. van Pée, A. Eychmüller, *Angew. Chem. Int. Ed.* **2008**, *47*, 7876.
[15] M. Park, C. Harrison, P. M. Chaikin, R. A. Register, D. H. Adamson, *Science* **1997**, *276*, 1401.
[16] R. Ruiz, H. Kang, F. A. Detcheverry, E. Dobisz, D. S. Kercher, T. R. Albrecht, J. J. de Pablo, P. F. Nealey, *Science* **2008**, *321*, 936.
[17] C. Tang, E. M. Lennon, G. H. Fredrickson, E. J. Kramer, C. J. Hawker, *Science* **2008**, *322*, 429.
[18] S. Park, D. H. Lee, J. Xu, B. Kim, S. W. Hong, U. Jeong, T. Xu, T. P. Russell, *Science* **2009**, *323*, 1030.
[19] C. T. Black, R. Ruiz, G. Breyta, J. Y. Cheng, M. E. Colburn, K. W. Guarini, H.-C. Kim, Y. Zhang, *IBM J. Res. Dev.* **2007**, *51*, 605.
[20] S.-J. Jeong, G. Xia, B. H. Kim, D. O. Shin, S.-W. Kang, S. O. Kim, *Adv. Mater.* **2008**, *20*, 1898.
[21] D. O. Shin, B. H. Kim, J.-H. Kang, S.-J. Jeong, S. H. Park, Y.-H. Lee, S. O. Kim, *Macromolecules* **2009**, *42*, 1189.
[22] S. H. Park, D. O. Shin, B. H. Kim, D. K. Yoon, K. Kim, S. Y. Lee, S.-H. Oh, S.-W. Choi, S. C. Jeon, S. O. Kim, *Soft Matter* **2010**, *6*, 120.
[23] B. H. Kim, D. O. Shin, S.-J. Jeong, C. M. Koo, S. C. Jeon, W. J. Hwang, S. Lee, M. G. Lee, S. O. Kim, *Adv. Mater.* **2008**, *20*, 2303.
[24] T. Thurn-Albrecht, J. Schotter, G. A. Kastle, N. Emley, T. Shibauchi, L. Krusin-Elbaum, K. Guarini, C. T. Black, M. T. Tuominen, T. P. Russell, *Science* **2000**, *290*, 2126.
[25] S. O. Kim, H. H. Solak, M. P. Stoykovich, N. J. Ferrier, J. J. de Pablo, P. F. Nealey, *Nature* **2003**, *424*, 411.
[26] I. Bita, J. K. W. Yang, Y. S. Jung, C. A. Ross, E. L. Thomas, K. K. Berggren, *Science* **2008**, *321*, 939.
[27] L. Wan, X. M. Yang, *Lanmuir* **2009**, *25*, 12408.
[28] X. M. Yang, L. Wan, S. Xiao, Y. Xu, D. K. Weller, *ACS Nano* **2010**, *3*, 1844.
[29] O. Hellwig, J. K. Bosworth, E. Dobisz, D. Kercher, T. Hauet, G. Zeltzer, J. D. Risner-Jamtgaard, D. Yaney, R. Ruiz, *Appl. Phys. Lett.* **2010**, *96*, 052511.
[30] S. Park, J.-Y. Wang, B. Kim, J. Xu, T. P. Russell, *ACS Nano* **2008**, *2*, 766.
[31] S. Park, B. Kim, O. Yavuzcetin, M. T. Tuominen, T. P. Russell, *ACS Nano* **2008**, *2*, 1363.
[32] S. Park, J.-Y. Wang, B. Kim, T. P. Russell, *Nano Lett.* **2008**, *8*, 1667.
[33] B.-H. Sohn, J.-M. Choi, S. I. Yoo, S.-H. Yun, W.-C. Zin, J. C. Jung, H. Kanehara, T. Hirata, T. Teranishi, *J. Am. Chem. Soc.* **2003**, *123*, 6368.
[34] M. Aizawa, J. M. Buriak, *Chem. Mater.* **2007**, *19*, 5090.
[35] J. Chai, D. Wang, X. Fan, J. M. Buriak, *Nat. Nanotechnol.* **2007**, *2*, 500.
[36] N. S. McIntyre, D. G. Zetaruk, *Anal. Chem.* **1977**, *49*, 1521.
[37] D. H. Lee, W. J. Lee, S. O. Kim, *Nano Lett.* **2009**, *9*, 1427.
[38] D. H. Lee, D. O. Shin, W. J. Lee, S. O. Kim, *Adv. Mater.* **2008**, *20*, 2480.
[39] D. H. Lee, J. E. Kim, T. H. Han, J. W. Hwang, S. Jeong, S.-Y. Choi, S. H. Hong, W. J. Lee, R. S. Ruoff, S. O. Kim, *Adv. Mater.* **2010**, *22*, 1247.
[40] S. Fan, M. G. Chapline, N. R. Franklin, T. W. Tombler, A. M. Cassell, H. Dai, *Science* **1999**, *283*, 512.
[41] Y.-T. Tseng, W.-H. Tseng, C.-H. Lin, R.-M. Ho, *Adv. Mater.* **2007**, *19*, 3584.